

Figure S1: Variation of the filling-in signal according to the averaged radiance of the GOSAT TANSO-FTS band 1; (a) P-polarization; (b) S-polarization. Filling-in signal over Antarctica, Greenland, cloudy ocean, and bare soil for January 2012 to December 2014 were used. Cloudy ocean data with a small variation in the TANSO-CAI radiance were used (Figs. S7 and S8). Bare soil data were identified in a similar way to the main text (Sect. 3.2). The bin size of the band 1 averaged radiance is $0.000002 \text{ V (cm}^{-1}\text{)}^{-1}$. The mean values are shown for bins with a standard error of the filling in signal $\leq 0.3 \times 10^{-9} \text{ W cm}^{-2} (\text{cm}^{-1})^{-1} \text{ sr}^{-1}$.

(a) P-polarization

(b) S-polarization

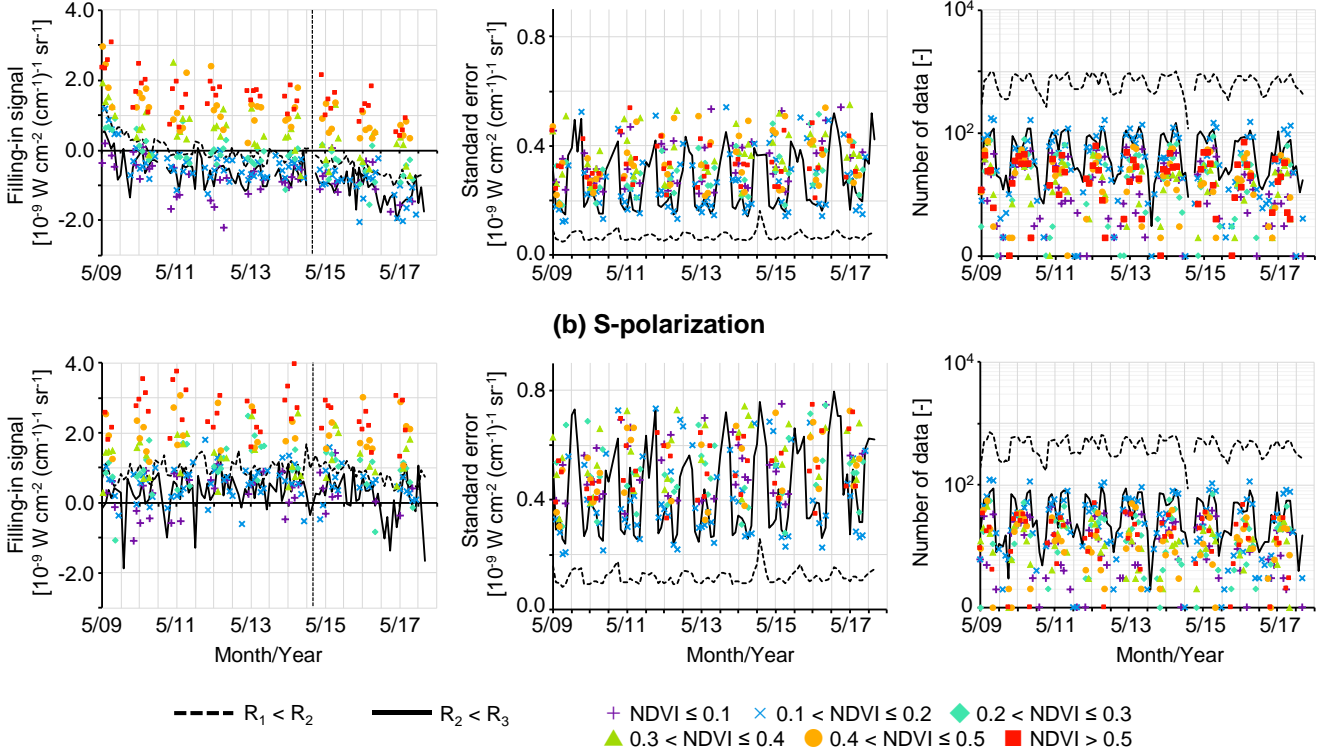
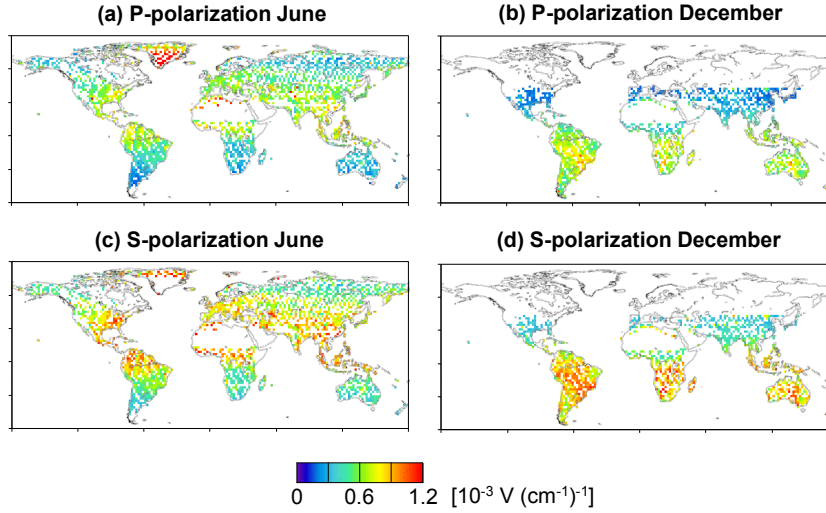


Figure S2: Variation of the monthly mean filling-in signal derived from data identified by the different criteria, albedo values (R_i for the TANSO-FTS band i) or NDVI values, within the latitude zone of 30°N to 45°N ; (a) averaged radiance of the TANSO-FTS band 1 P-polarization 0.0005 to $0.0006 \text{ V (cm}^{-1})^{-1}$; (b) S-polarization 0.0007 to $0.0008 \text{ V (cm}^{-1})^{-1}$. A vertical broken line indicates the change of the optics path selector (26 January 2015).

5

10



15 **Figure S3: Monthly mean of the averaged radiance of the GOSAT TANSO-FTS band 1 within a $2^\circ \times 2^\circ$ grid box for 2015; (a)(b) P-polarization; (c)(d) S-polarization; (a)(c) June; (b)(d) December. Only data with a cloud fraction ≤ 0.2 were used.**

20

25

30

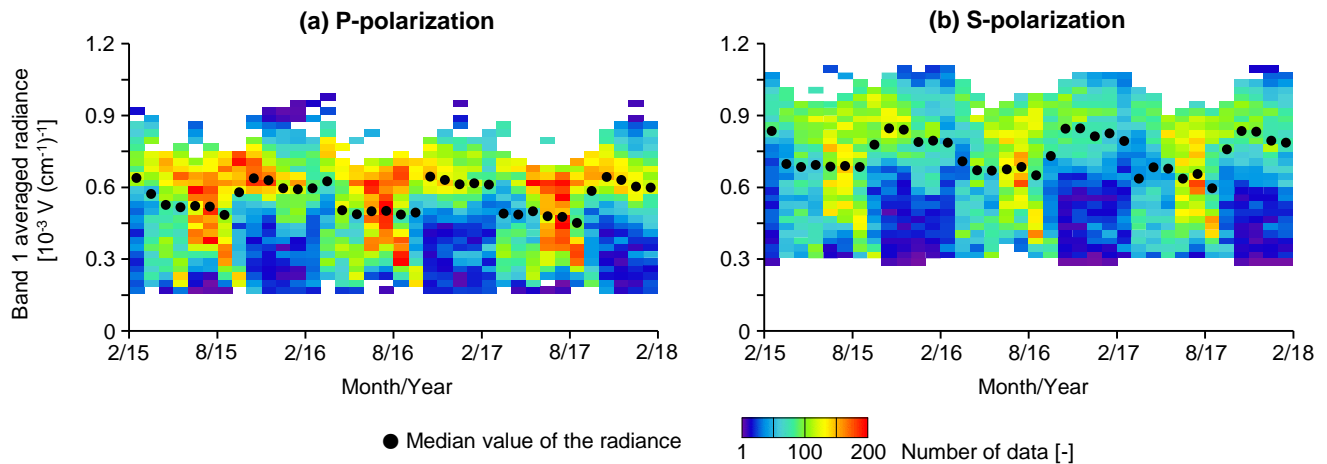


Figure S4: Frequency and median value of the band 1 averaged radiance for vegetated areas; (a) P-polarization; (b) S-polarization. The frequency was calculated with a bin size of $0.00003 \text{ V (cm}^{-1})^{-1}$. Observed data for forests (IGBP class number 1 to 5) were used. Method for assigning a land cover type to each footprint is described in Sect. 4.1. Only data with a cloud fraction ≤ 0.2 were used.

35

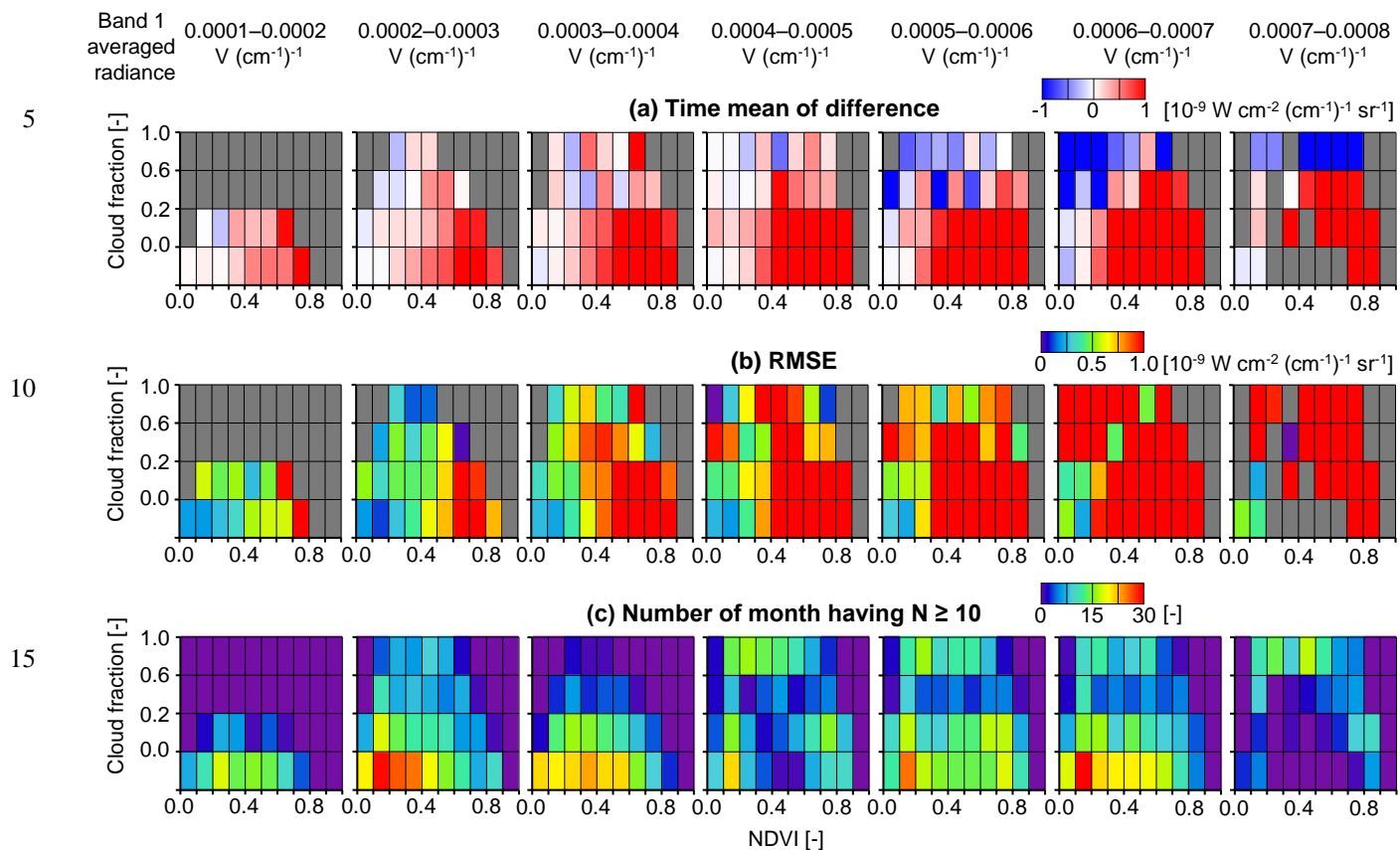


Figure S5: The difference in the monthly mean filling-in signal between data identified by various criteria (cloud fraction and NDVI) and the reference data (filling-in signal from each criteria — reference) was calculated for P-polarization; (a) the monthly value was averaged over 3 years (February 2015 to January 2018); (b) RMSE; (c) number of months where the number of data points (N) was more than 9. The calculation was conducted separately for the averaged radiance level of the TANSO-FTS band 1 ($0.0001 \text{ V (cm}^{-1}\text{)}^{-1}$ bin). Data included in the latitude zone of 30°N to 45°N were used. The reference data were identified by the criteria for bare soil determined in Sect. 3.3. Only data with a cloud fraction of 0 were used for the reference.

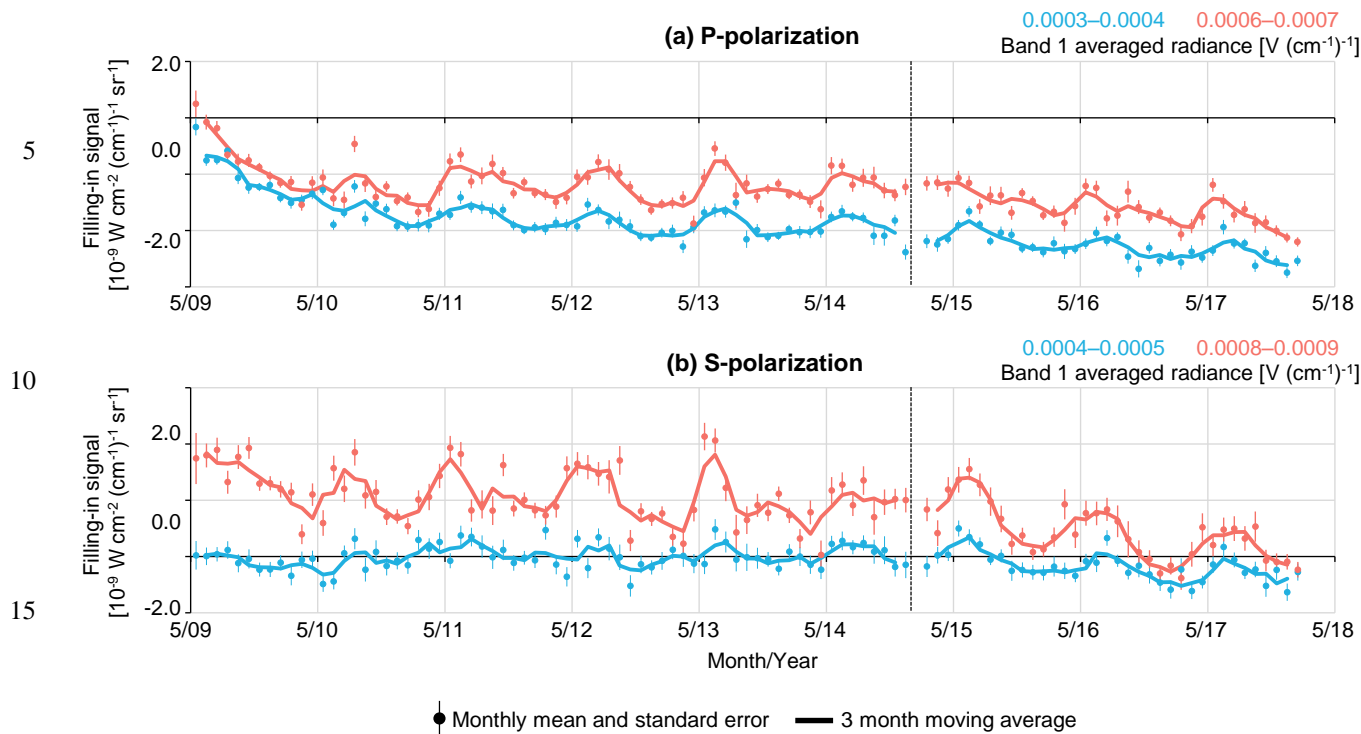


Figure S7: Temporal variation of the zero-level offset evaluated from cloudy ocean within the latitude zone of 30°N to 45°N; (a) P-polarization; (b) S-polarization. Results for different ranges of the observed radiance are depicted in each panel. Cloudy ocean data with a small variation in the TANSO-CAI radiance (cloud fraction > 0 and $VAR_{CAI} \leq 0.1$) were used since the filling-in signal varies according to the cloud fraction (Fig. S8). VAR_{CAI} is a ratio of the standard deviation to the mean value of the TANSO-CAI radiance within the TANSO-FTS IFOV. A vertical broken line indicates the change of the optics path selector (26 January 2015).

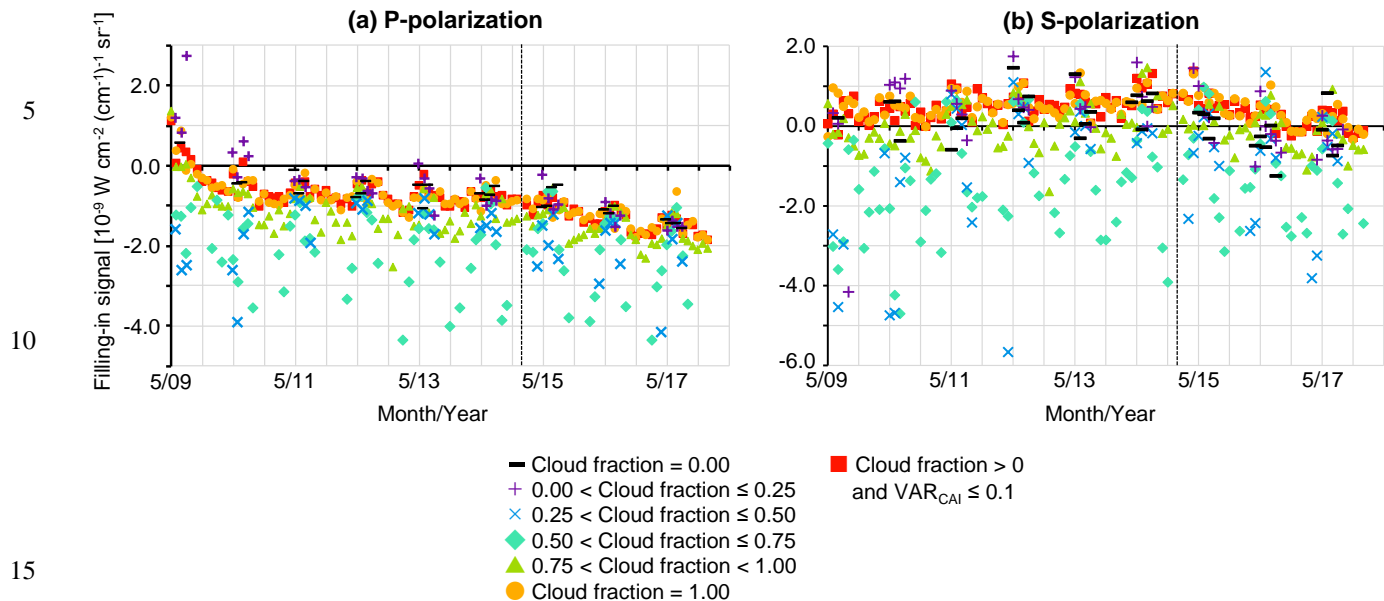


Figure S8: Variation of the monthly mean filling-in signal derived from the ocean data having different cloud fractions within the latitude zone of 30°N to 45°N; (a) averaged radiance of the TANSO-FTS band 1 P-polarization 0.0005 to 0.0006 $\text{V} (\text{cm}^{-1})^{-1}$; (b) S-polarization 0.0007 to 0.0008 $\text{V} (\text{cm}^{-1})^{-1}$. A vertical broken line indicates the change of the optics path selector (26 January 2015).

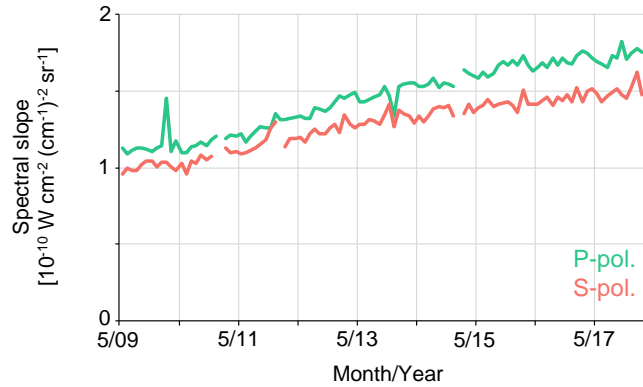


Figure S9: Temporal variation of the spectral slope of the TANSO-FTS band 1. Bare soil data identified by the criteria of $R_2 < R_3$ were used. Only data having band 1 averaged radiance between 0.000575 to $0.000625 \text{ V (cm}^{-1}\text{)}^{-1}$ and 0.000675 to $0.000725 \text{ V (cm}^{-1}\text{)}^{-1}$ were used for P- and S- polarization, respectively. Guanter et al. (2012) showed the spectral slope decreased with time. Difference in the version of L1 data and the correction of radiometric degradation seem to be reflected in the difference in spectral slope. Guanter et al. (2012) indicated that the temporal variation of the zero-level offset corresponds to that of spectral slope. In our results, for P-polarization, there seems to be a relationship between the zero-level offset and the spectral slope: time periods in which the zero-level offset decreased after GOSAT started observation and became stable correspond to the change in the spectral slope. However, the temporal variation of spectral slope is similar between P- and S-polarization unlike the zero-level offset. Difference in the zero-level offset correction in the L1 processing between L1 versions appears to affect the difference between Guanter et al. (2012) and our results. It is thought that both zero-level offset and spectral slope relate to the instrument characteristics, but there is no direct relationship between them.

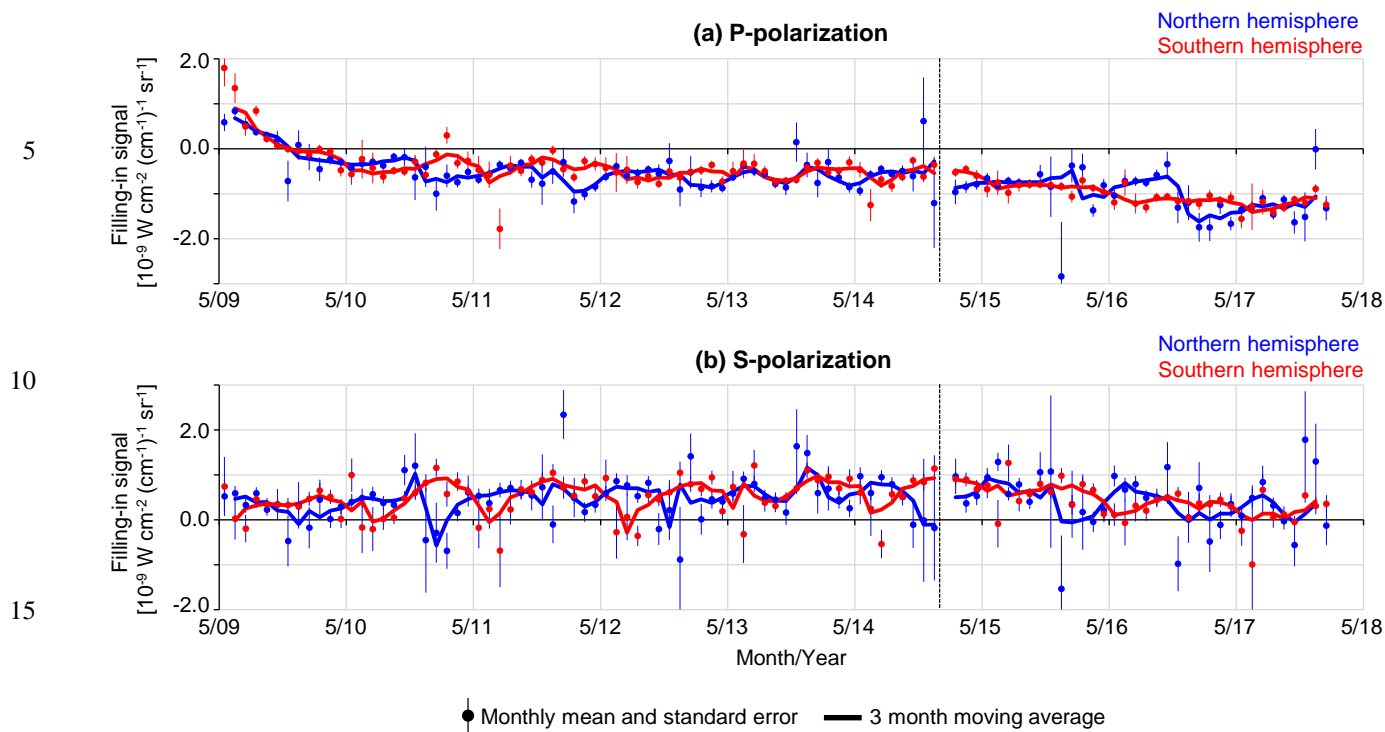


Figure S10: Temporal variation of the zero-level offset for the northern and southern hemisphere evaluated from bare soil; (a) averaged radiance of the TANSO-FTS band 1 P-polarization 0.0005 to 0.0006 $\text{V} (\text{cm}^{-1})^{-1}$; (b) S-polarization 0.0007 to 0.0008 $\text{V} (\text{cm}^{-1})^{-1}$. A vertical broken line indicates the change of the optics path selector (26 January 2015).

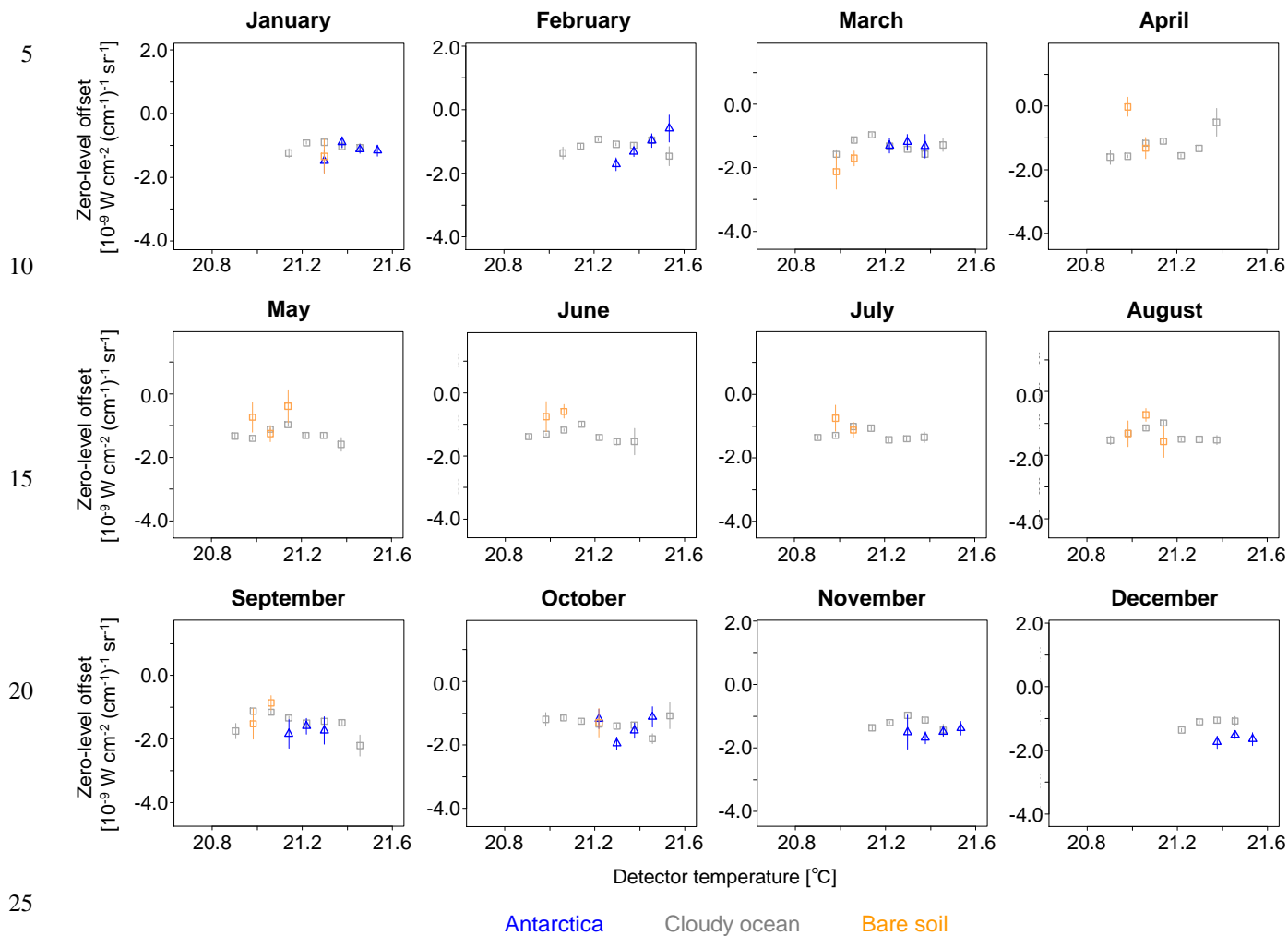


Figure S11: Variation of the filling-in signal according to the detector temperature for 2016 for P-polarization (0.0006 to 0.0007 V $(\text{cm}^{-1})^{-1}$). The detector temperature stored in the TANSO-FTS L1B product was used. The bare soil data were identified by the criteria determined in Sect. 3.2. Cloudy ocean data with a small variation in the TANSO-CAI radiance were used (Figs. S7 and S8).

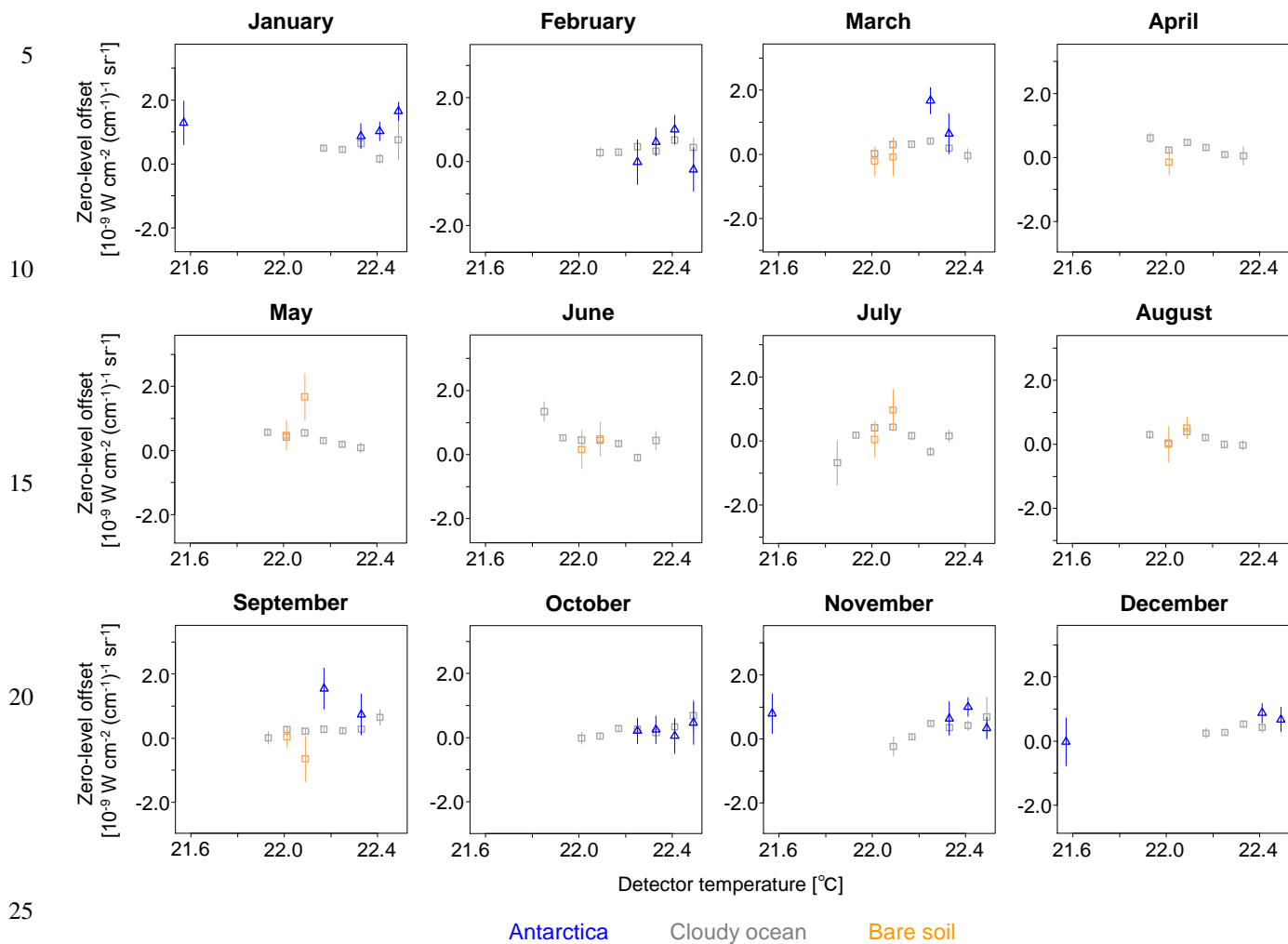
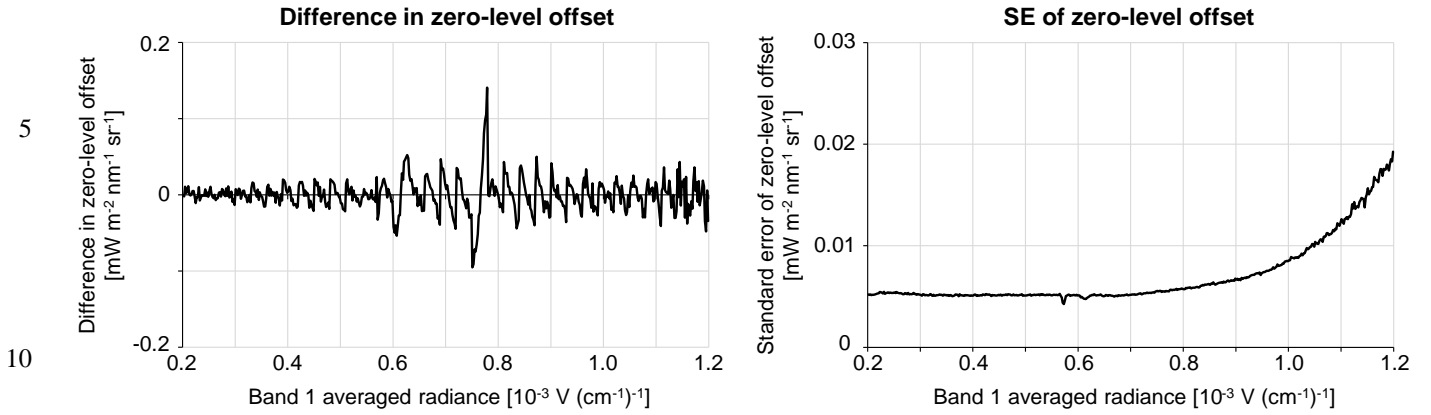


Figure S12: Similar to Fig. S11 but for S-polarization (0.0008 to $0.0009 \text{ V (cm}^{-1})^{-1}$).

(a) P-polarization



(b) S-polarization

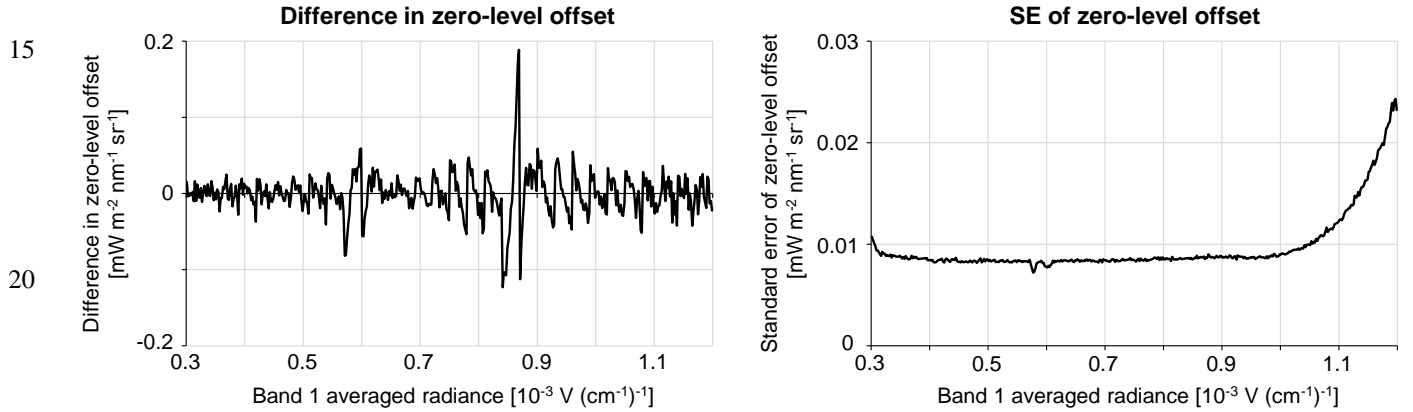


Figure S13: Difference in the zero-level offset according to the bin size of the band 1 averaged radiance; (a) P-polarization; (b) S-polarization. In each panel, difference in zero-level offset and standard error are presented. For the difference, the zero-level offset calculated with a bin size of $0.000002 \text{ (cm}^{-1})^{-1}$ was subtracted from that with $0.00003 \text{ V (cm}^{-1})^{-1}$. Standard error of the zero-level offset calculated with a bin size of $0.000002 \text{ (cm}^{-1})^{-1}$ is shown. The zero-level offset represented by a unit of SIF ($\text{mW m}^{-2} \text{ nm}^{-1} \text{ sr}^{-1}$) is shown in this figure. The same data as Fig. S1 was used.

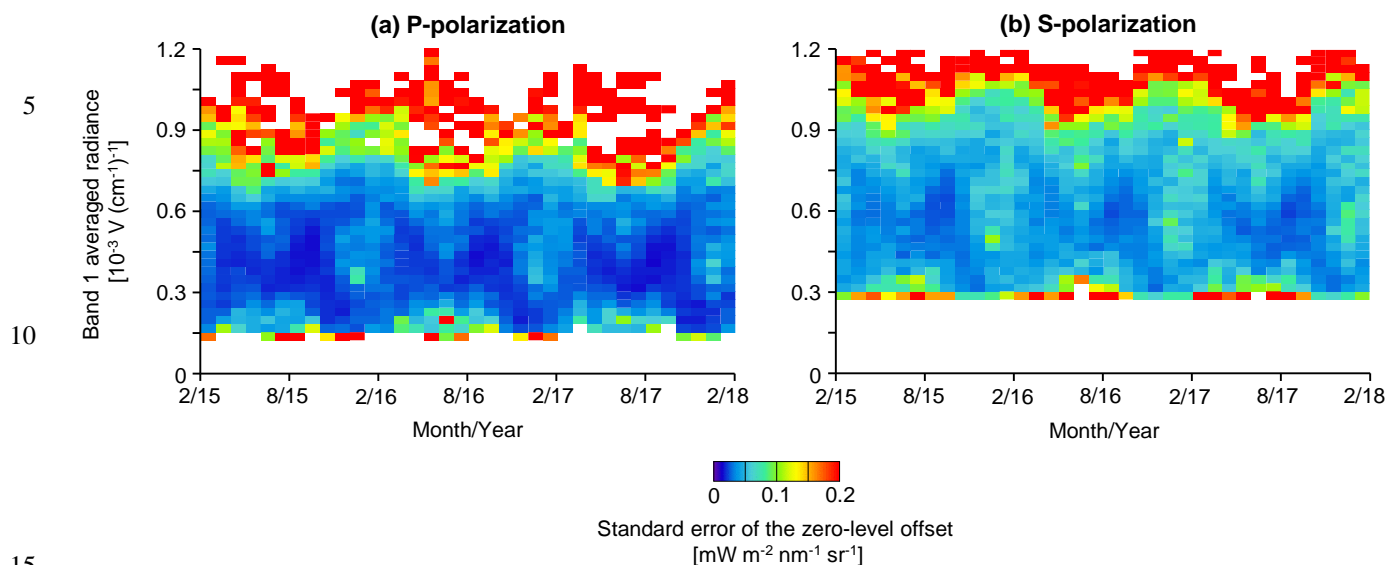


Figure S14: Standard error of the zero-level offset table.

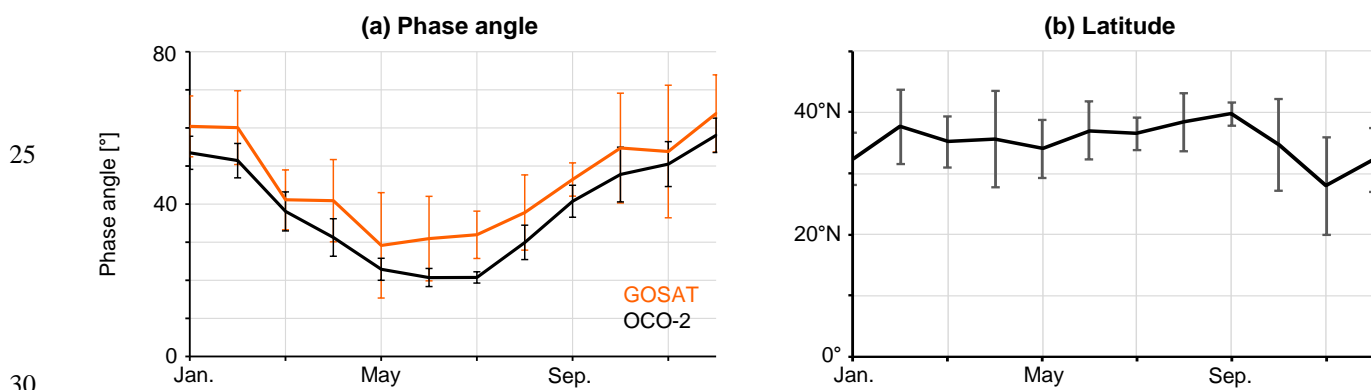
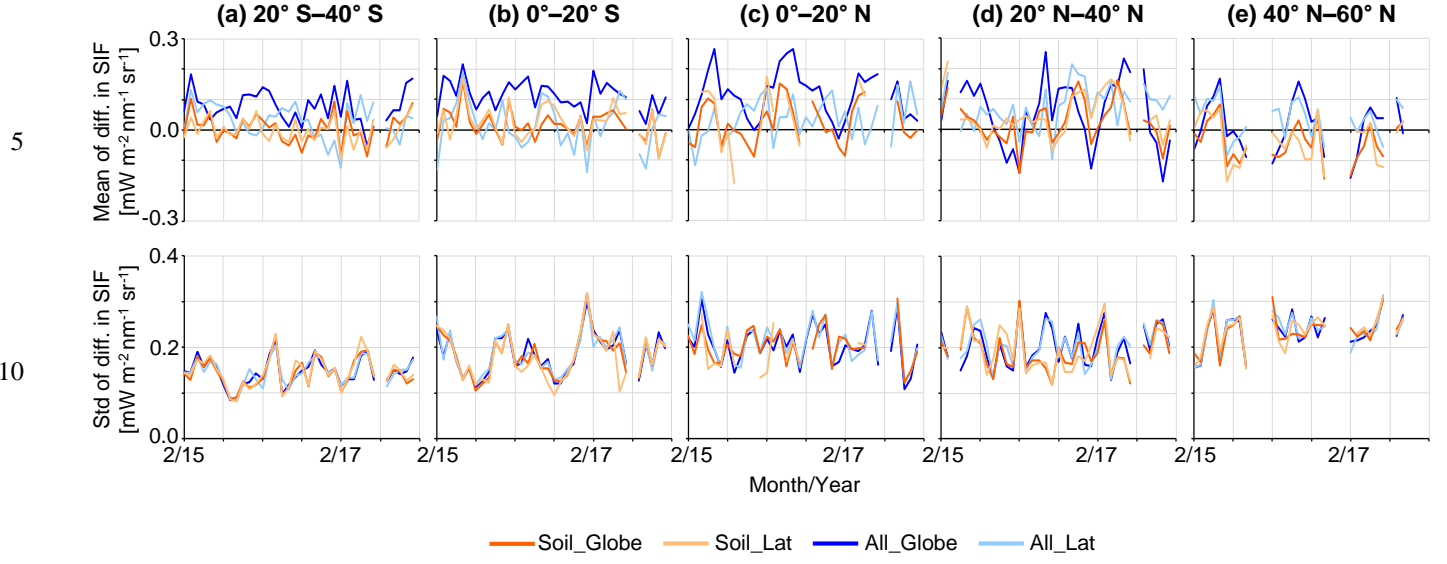


Figure S15: Temporal variation of phase angle and latitude of the GOSAT and OCO-2 data used in Sect. 4.2. Mean and standard deviation for each month was calculated without taking the year into account.



15 **Figure S16: Difference in the monthly mean SIF (GOSAT — OCO-2) within a $5^\circ \times 10^\circ$ grid box is averaged for each 20° latitude**
bin; (a)–(e) 20°S – 60°N with an interval of 20° . In each panel, the averaged value and the standard deviation of the difference in
each bin are presented. Results for different offset correction methods are presented; Soil_Globe: zero-level offset was evaluated
from bare soil over the globe (similar to the main text); Soil_Lat: similar to Soil_Globe but separately for the northern and the
 20 **All_Globe: zero-level offset was evaluated from Antarctica, Greenland, cloudy ocean, and bare soil;**
All_Lat: similar to All_Globe but separately for each latitude zone (15° interval) (similar strategy to that used by Joiner et al.
(2012)). Cloudy ocean data with a small variation in the TANSO-CAI radiance were used similar to Fig. S7. The difference in SIF
showed a seasonal cycle when the zero-level offset was evaluated from vegetation-free targets in both land and ocean and applied
 25 **over the globe (All_Globe). The zero-level offset had a seasonal cycle with a maximum around June for the northern hemisphere**
(the opposite of the cycle for the southern hemisphere). Correcting the offset separately for latitude zones (All_Lat) improved the
results. However, the amplitude of variation appears to be larger compared to Soil_Globe and Soil_Lat, indicating the possibility
that the cloudy ocean filling-in insufficiently accounts for the zero-level offset for land.

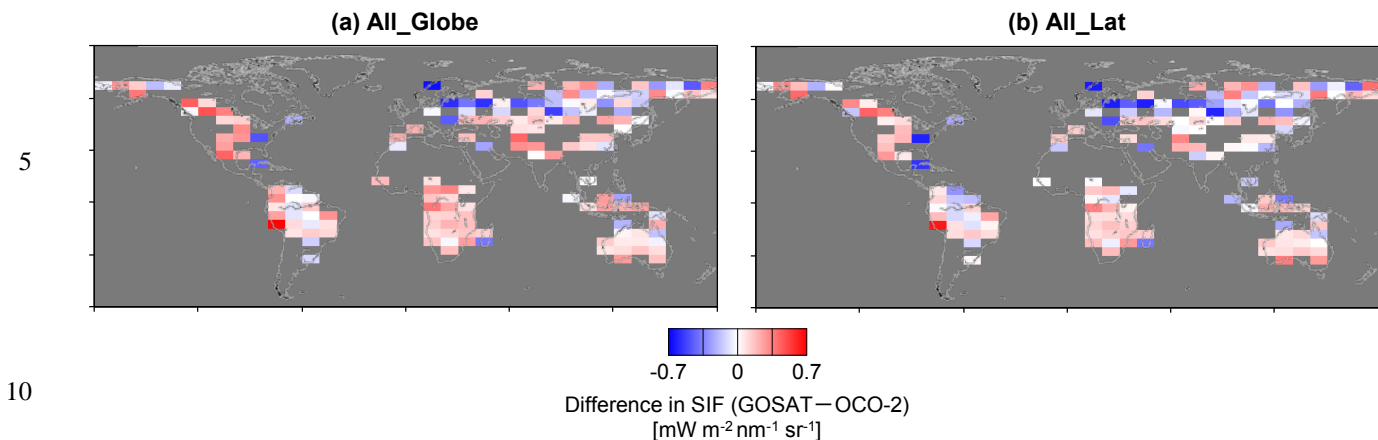


Figure S17: Difference in the monthly mean SIF (GOSAT — OCO-2) within a $5^\circ \times 10^\circ$ grid box for July 2015; (a) zero-level offset was evaluated from Antarctica, Greenland, cloudy ocean, and bare soil; (b) similar to (a) but separately for each latitude zone (15° interval). Only grids with more than 9 data points are depicted. For (a), GOSAT SIF was higher than OCO-2 SIF even for the latitude zone where the observation time was similar between the satellites. The difference in SIF became small when the zero-level offset correction was conducted separately for latitude zones (b). In this case, however, GOSAT SIF was higher than OCO-2 SIF at a difference in observation time of around -1.5 h (southern hemisphere), including the grids where OCO-2 SIF was almost zero (Fig. S18).

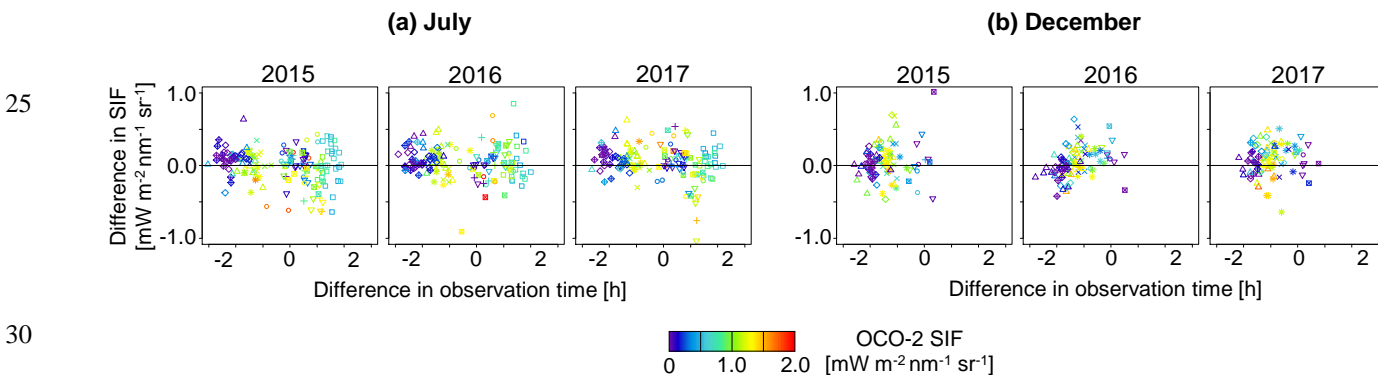


Figure S18: Relationship between the difference in SIF (GOSAT — OCO-2) and the difference in local time of the observation for 2015 to 2017; (a) July; (b) December. Results from the offset correction using data over Antarctica, Greenland, cloudy ocean, and bare soil separately for each latitude zone (15° interval) are presented. Each symbol represents a $5^\circ \times 10^\circ$ grid box.

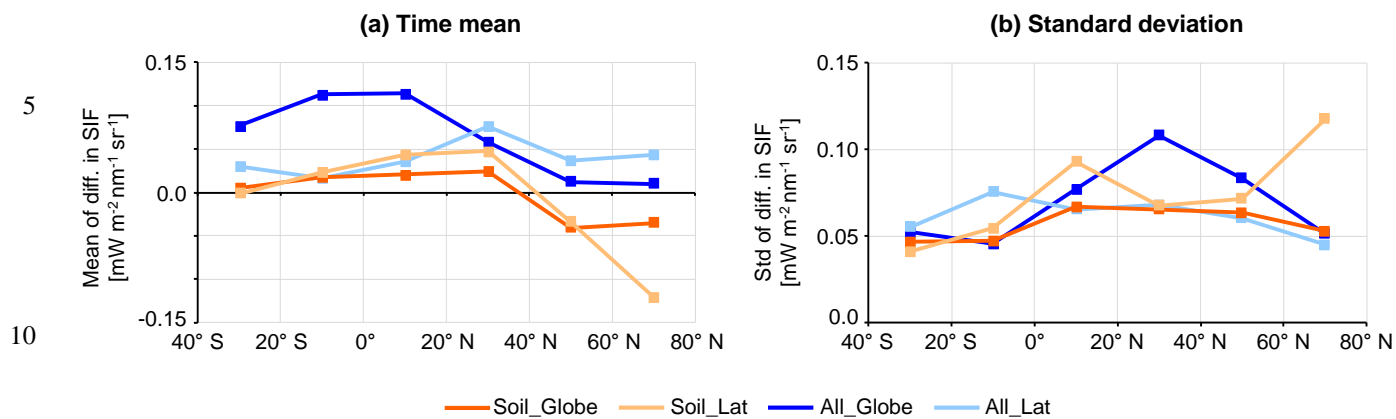


Figure S19: The monthly mean value shown in Fig. S16 is averaged over the target time period (February 2015 to January 2018); (a) averaged value; (b) standard deviation.